



**VICTORIA UNIVERSITY**  
MELBOURNE AUSTRALIA

*Environmental, economic, and serviceability attributes of residential foundation slabs: a comparison between waffle and stiffened rafts using multi-output deep learning*

This is the Published version of the following publication

Teodosio, Bertrand, Pallewela Liyanage, Piyal wasantha, Yaghoubi, Ehsan, Guerrieri, Maurice, Fragomeni, Salvatore and van Staden, Rudi (2023) Environmental, economic, and serviceability attributes of residential foundation slabs: a comparison between waffle and stiffened rafts using multi-output deep learning. *Journal of Building Engineering*, 80. ISSN 2352-7102

The publisher's official version can be found at  
<https://www.sciencedirect.com/science/article/pii/S2352710223021630>  
Note that access to this version may require subscription.

Downloaded from VU Research Repository <https://vuir.vu.edu.au/47593/>



ELSEVIER

Contents lists available at [ScienceDirect](https://www.sciencedirect.com)

## Journal of Building Engineering

journal homepage: [www.elsevier.com/locate/job](http://www.elsevier.com/locate/job)

# Environmental, economic, and serviceability attributes of residential foundation slabs: A comparison between waffle and stiffened rafts using multi-output deep learning

B. Teodosio<sup>a,c,\*</sup>, P.L.P. Wasantha<sup>a,b</sup>, E. Yaghoubi<sup>a,b</sup>, M. Guerrieri<sup>a,b</sup>,  
S. Fragomeni<sup>a,b</sup>, R. van Staden<sup>a,b</sup>

<sup>a</sup> Institute of Sustainable Industries & Liveable Cities, Victoria University, Melbourne, Victoria, 3011, Australia

<sup>b</sup> College of Engineering and Science, Victoria University, Melbourne, Victoria, 3011, Australia

<sup>c</sup> Energy Networks Australia, Melbourne, Victoria, 3000, Australia

## ARTICLE INFO

## Keywords:

Residential slabs  
Expansive soils  
Artificial intelligence  
Serviceability  
Life cycle cost  
Life cycle assessment  
Sustainable design

## ABSTRACT

The design of residential foundation slabs is commonly based on standards that emphasise the structural aspects and safety of the structure. Factors related to environmental and economic criteria are seldom given due consideration in the design phase. Considering the growing demand for sustainable approaches driven mainly by climate change concerns, this study developed a smart tool called Multi-Output Non-linear Design of Slabs (MOUNDS), which simultaneously predicts embodied energy, carbon emission, life cycle cost and deflection of waffle and stiffened rafts. MOUNDS considers the environmental, economic, and serviceability criteria of waffle and stiffened rafts on soils having varying reactivities. The standard deemed-to-comply design code for residential slabs and footings in Australia was investigated to determine the most advantageous foundation type in terms of both sustainability attributes and serviceability performances. The developed MOUNDS algorithm has shown accurate predictions. The predicted values of the: embodied energy of the residential slabs, greenhouse gas emission of the residential slabs, life cycle cost of the residential slabs, and maximum deflection of the residential slabs of waffle rafts were found more sustainable and serviceable than stiffened rafts in slight to moderate reactive sites. When sites are highly reactive, the difference between the environmental and economic of waffle rafts and stiffened rafts was minimal and did not conform to the serviceability limits of the Australian design code. This novel study linked and predicted the multi-disciplinary relationship between the environmental, economic and structural design aspects of residential slabs through machine learning. This is valuable in decision-making throughout the design phase considering the multi-faceted aspects of residential footing systems on reactive soils.

## Nomenclature

AEC	Architecture, engineering and construction
AI	Artificial Intelligence
$A_f$	area of residential slab

\* Corresponding author. Institute of Sustainable Industries & Liveable Cities, Victoria University, Melbourne, Victoria, 3011, Australia.  
E-mail address: [bteodosio@energynetworks.com.au](mailto:bteodosio@energynetworks.com.au) (B. Teodosio).

<https://doi.org/10.1016/j.job.2023.107983>

Received 5 July 2022; Received in revised form 19 September 2023; Accepted 19 October 2023

Available online 26 October 2023

2352-7102/© 2023 The Authors. Published by Elsevier Ltd. This is an open access article under the CC BY license (<http://creativecommons.org/licenses/by/4.0/>).

Adam	Adaptive moment estimation
AS	Australian Standards
BRAB	Building Research Advisory Board
$C_{fc}$	fixed cost
$C_{ic}$	indirect cost
CNN	Convolutional Neural Network
$D$	beam depth
DL	Deep Learning
EPiC	Environmental Performance in Construction
$EE_{LCI}$	Embodied energy of footing
GHG	Greenhouse gases
$GHG_{LCI}$	Greenhouse gas emission of footing
$EE_M, GHG_M, EE_T, GHG_T, EE_C, GHG_C, EE_D, GHG_D$	Lifecycle phases for materials, transportation, construction, and demolition for the embodied energy and greenhouse gas emission of footing
$H_s$	active depth zone
$h$	thickness
$I_{pb}, I_{ps}$	soil indices
ISO	International Organization for Standardization
$L$	footing span
LCI	Life Cycle Inventory
LCC	Life Cycle Cost
LRFD	Load and Resistance Factor Design
$L(y, \hat{y})$	Loss function
MOUNDS	Multi-Output Non-linear Design of Slabs
MSE	Mean Squared Error
$N$	number of soil layers or entries
$n_{sb}, n_{st}$	number of the bottom and top steel reinforcements
PTI	Post Tensioning Institute
$p, q$	Area and concentrated loads applied to the footing
ReLU	Rectified Linear Units
RMSprop	Root Mean Square Propagation
$size^{DL-1}$	size of the previous layer
$t_c$	construction duration
$V_{dw}, V_{db}, S_{dw}, \text{ and } S_{db}$	weights and biases that are calculated in iteration or epoch
$W$	footing width
WRI	Wire Reinforcement Institute
$w_i$	weight feature
$x_{min}$	minimum feature
$x_{max}$	maximum feature
$y$	true value
$\hat{y}$	predicted value
$y_s$	surface characteristic movement
$z$	depth from the ground to the middle of the soil layer
$\alpha$	lateral restraint factor
$\beta_1 \text{ and } \beta_2$	decay rates
$\Delta_a$	allowable differential footing deflection based on AS 2870 (Design of residential slabs)
$\Delta_{max}$	maximum differential footing deflection (in this study considering x, y, and z directions)
$\Delta \bar{u}$	averaged soil suction
$\epsilon_{ms}$	shrink-swell parameter
$\lambda$	hyperparameter for regularisation
$\phi_{sb}, \phi_{st}$	diameter of bottom and top steel reinforcements
$\phi_m$	diameter of mesh reinforcement

## 1. Introduction

### 1.1. Background of the study

The architecture, engineering and construction (AEC) industries contribute to more than 40% of global energy consumption and more than 30% of the overall greenhouse gas (GHG) emissions [1]. The growing demand for new residential structures due to the

increase in population and immigration will necessitate these industries to build adequate and sustainable dwellings [2]. These challenges compel the AEC sectors to deliver efficient, long-term and cost-effective solutions with safe and sustainable considerations [3]. Quantitative data presented by the United Nations Environment Program [4] have shown that material extraction, manufacturing and transportation, construction, maintenance and demolition, known as the embodied phase, contribute 10%–20% of the environmental impacts related to energy and GHG emission. This contribution increases to more than 50% for low-energy buildings like single-detached dwellings. The construction of residential foundation slabs is specifically a primary consideration due to the faster rate of GHG emission from activities such as earthmoving [5]. Note that residential foundation slabs are termed as residential slabs hereafter in the research. However, these environmental aspects are unfortunately overlooked in the design of residential slabs by many standards, for instance, the Australian Standard (AS) 2870 by Standards Australia [6] for residential slabs and footings. Thus, this study aims to investigate the link between the environmental, economic and structural design aspects of residential slabs and predict these sustainability aspects through deep learning (DL) algorithms.

### 1.2. Residential footings and soil movement challenges

Common residential slabs can be classified into four types; these are (1) basements (2) raft slabs, (3) strip footings, and (4) stumps [7]. Basements are internal and external perimeter walls on slabs [8]. Raft slabs are concrete flat substructures constructed on the ground with internal and edge beams [9]. Strip footings, on the other hand, are linear strips of concrete placed into a trench or formwork directly supporting load-bearing walls [6]. Stumps are residential slabs that support suspended floors [7].

In the design of the above residential slabs, considerations are given to the soil bearing capacity, structural load capacity, maximum settlement and differential ground movement [10]. Different design philosophies against the failure of residential slabs can be adopted; these include the overall factor of safety approach, the partial factor of safety approach, the limit state design or Load and Resistance Factor Design (LRFD) approach, and the probabilistic approach [11]. In most cases, the serviceability of footings related to settlement often controls the design, in particular for shallow foundations and foundations on clayey soils.

The behaviour of clayey soils has been extensively studied in the literature primarily due to their problematic nature caused by the lower mechanical strength when wet [12,13] and the potential for significant volume change based on the water content, commonly known as reactivity [14,15]. Reactive soils are found in many countries around the world, including Argentina, Australia, Brazil, Canada, China, Egypt, Ethiopia, India, Iran, Malaysia, Mexico, South Africa, Spain, Turkey, the United Kingdom, and the United States of America, [16,17]. The reactive soils swell due to moisture content increase and shrink due to moisture content decrease [9,18]. The swelling and shrinking of the ground could damage structures, particularly lightweight structures such as pavements, underground pipes, and residential structures [19–21]. The cumulative repair expenditures due to such damage is more than twice the loss incurred from natural disasters like floods, hurricanes, tornadoes, and earthquakes in the United States [22].

Several residential slab design methods for construction on reactive soils have been developed [23]. The Building Research Advisory Board [24] proposed the BRAB method, which has a simple approach and yields a more conservative design [25]. Snowden [26] improved the BRAB method and developed the Wire Reinforcement Institute (WRI) method, an empirical technique that calculates the required dimensions of residential footings more conservatively. Lytton [27] created a procedure that uses beam-on-mound equations and coupled springs. This method was then modified by Walsh and Walsh [28] and Mitchell [29] to propose improved methods. The Post Tensioning Institute (PTI) [30] developed an empirical design approach using water balance, soil diffusion, and soil particle size, known as the PTI Method.

### 1.3. The Australian context

The Australian Standard 2870 (AS 2870-2011) was developed by Standards Australia [6] to specify the required performance criteria and designs of residential slabs for sites with less reactive to highly reactive soils that are susceptible to substantial shrinking and swelling ground movements. This standard is primarily based on the methodologies of Walsh and Walsh [28] and Mitchell [29] and was created by performing parametric analyses [9].

Two approaches are presented in AS 2870-2011 to design residential slabs and footings, being deemed-to-comply design method, and maximum differential deflection method. The first approach follows the standard deemed-to-comply designs for stiffened rafts, waffle rafts, and strip footings depending on the site classification. The site classification can be determined by either identifying the soil borehole profile or estimating the characteristic surface movement ( $y_s$ ) of the subsurface soil using Equation (1),

$$y_s = \frac{1}{100} \sum_{n=1}^N (I_{pt} \Delta \bar{u} h)_n \quad (1)$$

where  $\Delta \bar{u}$  is the averaged soil suction,  $h$  is the thickness of the considered layer,  $N$  is the number of soil layers, and  $I_{pt}$  is the instability index described as

$$I_{pt} = \alpha I_{ps} \quad (2)$$

where  $I_{ps}$  is the shrinkage index and  $\alpha$  is the lateral restraint factor with the value taken for the layers in the cracked zone as 1.0 or the layers in the uncracked zone calculated as

$$\alpha = 2 - \frac{z}{5} \quad (3)$$

where  $z$  is the depth to the middle of the soil layer from the finished ground level.

The sites are classified as A, S, M, H1, H2, E and P [6]. Sites with a design depth of soil suction change ( $H_s$ ) equal to or greater than 3 m are considered sites with deep-seated moisture changes that can be classified as M-D, H1-D, H2-D or E-D. These sites are commonly located in dry climates with corresponding  $H_s$  equal to or greater than 3 m in depth. Table 1 summarises the criteria for the above-mentioned classification scheme.

The standard-design procedure based on the site classification specified in AS 2870 -2011 only applies to Classes A, S, M, M-D, H1, H1-D, H2 and H2-D, depending on the type of residential slab being designed. In addition, these deemed-to-comply designs shall not have a footing length greater than 30 m and a structure height more than 8.5 m [6].

The second design method can be followed if the standard deemed-to-comply designs do not meet the criteria specified in AS 2870-2011. In this approach, the design should satisfy the maximum differential deflection of the residential slabs ( $\Delta_{max}$ ) based on the form of construction specified in Table 2. In the absence of information, the serviceability limit shall be taken as the lesser of the two values between the maximum differential deflections as a function of span and the specified differential deflection limits in Table 2.

A comparison of design methods for residential slabs was conducted by Abdelmalak [25] and Teodosio et al. [23] using the second design method of AS 2870-2011. The comparison revealed that maximum differential deflection method, together with the Walsh Method and Mitchell method, tend to calculate lower structural dimension requirements than the aforementioned design approaches such as the BRAB, WRI, and PTI Methods. This may be critical in areas with higher reactive soil movement, since more conservative design methods can accommodate higher values of  $y_s$  [31]. Therefore, a re-evaluation of the design philosophy is imperative to achieve a more serviceable substructure. In addition, the integration of economic and environmental factors into the design process will lead to more practical and sustainable residential slabs compared to the current practice.

#### 1.4. Application of artificial intelligence in reactive soil

The application of Artificial Intelligence (AI) in geotechnical has been observed since early 1980s. The applications were limited due to the restricted computing technologies, data availability, storage. This steadily increased in the late 2010s. The application of AI is specifically useful for soil analyses due to its anisotropic and arbitrary behaviour. Early application of AI techniques to geotechnical engineering used expert systems, fuzzy logic, and pattern recognition for assessing abutments, landslide, building foundation, and mines (Adams et al., 1989; Gupta and Bodechtel, 1982; Scoble et al., 1986; Wong et al., 1989). This was extended to the use of an artificial neural network (ANN), hybrid expert systems, and image analysis of soil parameters and geo-structures (Chan et al., 1995; Kayen et al., 1999; Maher and Williams, 1991; Oliphant, 1999). The progress in computing, data availability, and storage increased the application of AI to hazard mitigation, geo-structural health monitoring, and nanotechnology using Deep Learning (DL) and Convolutional Neural Network (CNN), clustering, hybrid genetic algorithms, and fuzzy logic (Abbas Abbaszadeh Shahri, 2016; Amezcuita-Sanchez et al., 2016; Congress and Puppala, 2020; Kadivar et al., 2011).

In geotechnical engineering, clay has observed noteworthy interest due to its lower mechanical strength compared to other types of soil. This is specifically true in wetter states causing larger volumetric variations due to changes in moisture content (Ural, 2018). Clayey soils can be found in many areas such as the United States of America, Canada, Mexico, Guatemala, Venezuela, Colombia, Peru, Bolivia, Venezuela, Brazil, Argentina, the United Kingdom, Spain, Egypt, Sudan, Ethiopia, Turkey, India, China, Malaysia, and Australia. Most clayey soils are reactive, which undergo significant volume changes due to variation in soil water content, leading to ground swelling when their water content increases and shrinking when their water content decreases [2]. Such swelling and shrinking behaviour induce damage to lightweight structures such as pavements, underground pipes, and residential structures (Johnson, 1969; [15,19]). Reactive soils induced distress to physical infrastructures have been reported globally, including Australia, China, Egypt, India, Israel, South Africa, the United Kingdom, and the United States of America, resulting in significant socio-economic impact (Li et al., 2014). Infrastructure rehabilitation and construction expenditures is more than twice the loss incurred from natural disasters such as floods, hurricanes, tornadoes, and earthquakes as a result of soil movements [22].

The challenges due to reactive soils require complex multi-physical non-linear analysis for a heterogeneous and anisotropic soil layers. The application of AI algorithms to reactive soils can allow the processing of big data to build non-linear models and predict more insightful outcomes (Theodoridis, 2020). The first recorded AI application to reactive soil was conducted by Hallaire (1993). This

**Table 1**  
Site classification based on soil reactivity [6].

Site Class	Foundation	Expected $y_s$ (mm)
A	Sand and rocks without ground movement	0
S	Slightly reactive foundation with low clay or silt portion	$0 < y_s \leq 20$
M	Moderately reactive foundation with clay or silt	$20 < y_s \leq 40$
M-D	Moderately reactive foundation with clay or silt and $H_s \geq 3$ m	$20 < y_s \leq 40$
H1	Highly reactive foundation	$40 < y_s \leq 60$
H1-D	Highly reactive foundation and $H_s \geq 3$ m	$40 < y_s \leq 60$
H2	Very highly reactive foundation	$60 < y_s \leq 75$
H2-D	Very highly reactive foundation and $H_s \geq 3$ m	$60 < y_s \leq 75$
E	Extremely highly reactive foundation	$y_s > 75$
E-D	Extremely highly reactive foundation and $H_s \geq 3$ m	$y_s > 75$
P	Soft or unstable foundations, soft clay, loose sands, landslip, mine subsidence, collapsing soils, erosion prone, reactive soil subjected to abnormal moisture conditions (soil suction variation $>1.2$ pF)	-

**Table 2**  
Allowable differential footing deflection ( $\Delta_a$ ) for the design of footings and rafts [6].

Form of construction	Maximum differential deflections as a function of span (mm)	Specified differential deflection limits (mm)
Clad frame	L/300	40
Articulated masonry veneer	L/400	30
Masonry veneer	L/600	20
Articulated full masonry	L/800	15
Full masonry	L/2000	10

is ten years after the first AI application in geotechnical engineering. Applications of AI in reactive soil research were related to soil characterisation and strength prediction, soil and structure performance, clay cracking and desiccation, and soil movement and stabilisation (Gong et al., 2004; Huang et al., 2019; Mahfouz et al., 2007; Shengquan et al., 2015; Yin et al., 2018). These implemented AI techniques such as artificial neural networks (ANN), support vector machine (SVM), genetic algorithms (GA), fuzzy logic, and image analysis (Congress and Puppala, 2020; Das et al., 2010; Julina and Thyagaraj, 2019; Mozumder and Laskar, 2015; Samui et al., 2011). Despite these AI applications, AI's potential is not fully utilised to study reactive soils.

### 1.5. Objectives and framework

The most common types of residential slabs in Australia are the waffle raft and the stiffened raft accounting for around 65% of the new and existing single-detached dwellings [32]. Slab structures, such as waffle rafts and stiffened rafts, have been commonly used as suitable residential slabs for lightweight structures on reactive soils due to the uniform distribution of applied loads from the superstructure and the pressure from the swelling ground [33]. This could be the reason why AS 2870-2011 presents standard deemed-to-comply designs for both waffle rafts and stiffened rafts dependent on the site classification (Table 1) and form of construction (Table 2). In recent years, a great demand for houses has been observed in Australia due to the increasing population and immigration. In 2016, the number of recorded new dwellings was around 71,000, which proliferated to approximately 134,000 in 2021 [32]. Most of these new dwellings have residential slabs designed based on the standard deemed-to-comply design approach of AS 2870-2011. In this study, a Multi-Output Non-linear Design of Slabs (MOUNDS) algorithm is developed that predicts the embodied energy, carbon emission, life cycle cost and deflection of waffle rafts and stiffened rafts based on the provided deemed-to-comply designs in AS 2870. Thereby providing a multi-faceted approach for sustainable design of residential slabs on reactive soils. MOUNDS enables simultaneous consideration of the environmental, economic and serviceability aspects of residential slabs. These sustainability, economic, and serviceability attributes of waffle and stiffened rafts are compared to provide necessary insights for prospective homeowners and building professionals to choose the safer, more practical and more sustainable option of residential slabs.

## 2. Methodology

The multi-faceted smart estimator, MOUNDS, was developed using DL algorithms that incorporates sustainability aspects in residential slabs design. MOUNDS simultaneously predicts four target outputs as listed below.

- the embodied energy of the residential slabs,  $EE_{LCI}$ ,
- the greenhouse gas emission of the residential slabs,  $GHG_{LCI}$ ,
- the life cycle cost of the residential slabs,  $LCC$ , and
- the maximum deflection of the residential slabs,  $\Delta_{max}$ .

The developed multi-output DL model can be used to compare the widely used waffle rafts and stiffened rafts based on the standards deemed-to-comply designs in AS 2870. The methodologies to calculate the target outputs are discussed in this section, along with the datasets and MOUNDS.

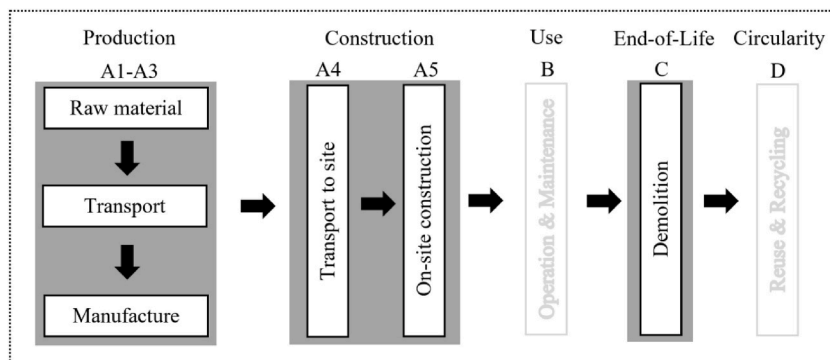


**Fig. 1.** Life-cycle analysis system boundary for waffle rafts and stiffened rafts (modified after Comité Européen De Normalisation [36]).

2.1. Life cycle inventory for the embodied energy and GHG emission

Life-cycle inventory (LCI) was used to estimate the environmental impacts of the most commonly used residential slabs in Australia (i.e. waffle rafts and stiffened rafts) based on [34,35]. The LCI assists in investigating opportunities for improvements in product sustainability and addresses the estimation of environmental impacts throughout the life cycle of a product [35]. The functional units in the current study were the  $EE_{LCI}$  in GJ, and  $GHG_{LCI}$  in ton, for the whole waffle rafts and stiffened rafts. The life cycle system boundary was investigated from cradle-to-grave, as shown in Fig. 1, which was adopted from EN 15978 by Comité Européen De Normalisation [36]. The life cycle stages of production (A1–A3), transport to the site (A4), construction (A5), and demolition (C) were taken into account, leaving out the operation and maintenance and reuse and recycling stages (B and D), which are out of the scope of this study.

The estimation of  $EE_{LCI}$  and  $GHG_{LCI}$  was based on the system boundary in Fig. 1 and calculated using Equations (4) and (5),

$$EE_{LCI} = EE_M + EE_T + EE_C + EE_D \tag{4}$$

$$GHG_{LCI} = GHG_M + GHG_T + GHG_C + GHG_D \tag{5}$$

where  $EE_M$  and  $GHG_M$  are the total embodied energy and greenhouse gas of materials and components,  $EE_T$  and  $GHG_T$  are the total embodied energy and greenhouse gas emission due to transportation,  $EE_C$  and  $GHG_C$  are the total embodied energy and greenhouse gas emission of due to construction,  $EE_D$  and  $GHG_D$  are the total embodied energy and greenhouse gas emission due to demolition.

The main resources used for LCI calculations were the EPiC database by Crawford et al. [37], the Australian National LCI (AusLCI) database by Grant [38], and the study conducted by Teodosio et al. [3]. The distance from the concrete batching plant, steel manufacturing plant, and excavator to the construction site was taken as 50 km, a common assumed distance based on an interview with practicing professionals, to quantify the  $EE_T$  and  $GHG_T$ . The concrete wastage was specified to be 15%, in accordance with the practice of builders and contractors [37].

The values of  $EE_{LCI}$  and  $GHG_{LCI}$  were calculated using the energy and carbon emission factors listed in Table 3. Sample calculations are presented in Table A1 and Table A2 for waffle rafts and stiffened rafts in an H2 site, respectively.

2.2. Life cycle cost analysis

The values of LCC of waffle rafts and stiffened rafts were calculated using ISO [39], considering the construction cost. This study assumed that the operation, occupancy and disposal costs are negligible for lightweight structures such as single-detached dwellings. The LCC was calculated using Equation (6).

$$LCC = C_{fc} + \sum C_{dc}A_f + \sum C_{ic}t_c \tag{6}$$

where  $C_{fc}$  is the fixed cost,  $C_{dc}$  is the direct cost proportional to the area of the residential slab  $A_f$ ,  $C_{ic}$  is the indirect cost proportional to the construction period, and  $t_c$  is the duration of the construction. The primary resource used for the different material and labour costs was Rawlinsons [40]. Supplementary data from case studies, quotes and estimates were used when data were inaccessible in the cost guide of Rawlinsons [40]. Example calculations are presented in Table A3 for a waffle raft and Table A4 for a stiffened raft considering an H2 site.

2.3. Serviceability analysis using a hydro-mechanical model

Parametric simulations were performed using the hydro-mechanical Finite Element Model developed by Teodosio [2] using ABAQUS [41]. Simulations were conducted for both waffle rafts and stiffened rafts with varying soil, structural, and environmental

**Table 3**  
Sample LCI for a waffle raft constructed on an H2 site with articulated masonry veneer ( $A_f = 300 \text{ m}^2$ ).

Item	Description	Unit	Qty	Embodied Energy, $EE_{LCI}$		Greenhouse Gas, $GHG_{LCI}$	
				Rate (GJ)	Amount (GJ)	Rate (tonCO <sub>2</sub> )	Amount (tonCO <sub>2</sub> )
<b>A</b>	<b>Materials</b>						
A1	20 MPa concrete	m3	36.37	0.1760	6.4014	0.3390	12.3299
A2	Steel reinforcement	t	1.35	48.7000	65.6415	0.0029	0.0039
A3	Waffle pod EPS	kg	35.61	0.0830	2.9554	0.0006	0.0217
A4	Sand subgrade	m3	30.00	0.2600	7.8000		
<b>B</b>	<b>Transportation</b>						
B1	Concrete	m3	36.37	0.1980	7.2016	0.0058	0.2096
B2	Steel	kg	1.35	0.0010	0.0013	0.0000	0.0000
B3	Excavator in/out	km	100.00	0.0180	1.8000	0.0013	0.1271
B4	Waffle pod (EPS) delivery	kg	35.61	0.0010	0.0356	0.0000	0.0010
<b>C</b>	<b>On-site construction</b>						
C1	Excavator (0.2 m <sup>3</sup> bucket)	h	8.82	0.1080	0.9529	0.0131	0.1158
C2	Concrete pump	h	0.79	0.5400	0.4270	0.0461	0.0365
<b>D</b>	<b>End-of-life</b>						
D1	Demolition	t	77.49	0.0070	0.5424	0.0005	0.0418
<b>Total</b>					<b>93.76</b>		<b>12.89</b>

parameters. These simulations were divided based on the shrinking and swelling movement of reactive soils; (1) waffle rafts on the shrinking ground, (2) waffle rafts on the swelling ground, (3) stiffened rafts on the shrinking ground, and (4) stiffened rafts on the swelling ground. The target output was  $\Delta_{max}$ , and the input features were based on the general principles outlined in AS 2870.4.6 by Standards Australia [6] as follows:

- characteristic surface movement or the maximum ground movement,  $y_s$ ,
- beam depths,  $D$ ,
- area of the residential slabs ( $A_f$ ) based on  $L$  and  $W$ ,
- number of the bottom and top steel reinforcements,  $n_{sb}$  and  $n_{st}$ ,
- bottom and top steel reinforcement,  $\varnothing_{sb}$  and  $\varnothing_{st}$ ,
- mesh reinforcement diameter,  $\varnothing_m$ ,
- area and loads applied to a stiffened raft or a waffle raft,  $p$  and  $q$ ,
- active depth zone,  $H_s$ , and
- shrink-swell parameter,  $\varepsilon_{ms}$ .

#### 2.4. Datasets for the multi-output DL algorithm

The values of  $EE_{LCl}$ ,  $GHG_{LCl}$ ,  $LCC$  and  $\Delta_{max}$  were calculated with varying values of the input features within a given range. The total number of data entries for waffle rafts and stiffened rafts were 3120 and 7020 for waffle rafts and stiffened rafts, respectively. This difference in number is because of the difference in specifications for waffle rafts and stiffened rafts in the deemed-to-comply design specified in AS 2870. Some specifications in waffle rafts are similar or overlapping with specifications in another site classification or form of construction. For instance, a construction with articulated masonry veneer on a Class S site has the same deemed-to-comply design as that of a Class M site with the same form of construction for waffle rafts. In the deemed-to-comply stiffened raft designs, such overlapping cases are minimal.

The datasets for waffle rafts and stiffened rafts were split into training, validation and testing sets with a ratio of 60% training, 20% validation and 20% testing as recommended by data science practice [42]. The validation set was used during the training phase of the deep learning model to provide an unbiased evaluation of its performance and to fine-tune the model's parameters. On the other hand, the test set was used after the model has been fully trained to assess its performance on completely unseen data. The splitting of dataset resulted into training sets of 1872 for waffle rafts and 4212 for stiffened rafts. The final data entries for the validation and testing set were 624 for the waffle raft and 1404 for the stiffened raft. The range of values of each parameter is presented in Table 4.

#### 2.5. Development of the multi-output deep learning algorithm

MOUNDS was used to obtain the acceptable weights for the prediction of  $EE_{LCl}$ ,  $GHG_{LCl}$ ,  $LCC$  and  $\Delta_{max}$ . The DL algorithm had an input layer, five hidden layers with 256 units, and an output layer, as illustrated in Fig. 2. This deep learning architecture was determined by trial and error and was observed to produce acceptable results. The input layer contains the input vector extracted from AS 2870-2011 dependent on the deemed-to-comply design specifications, as shown in Table 4.

The DL algorithm for waffle rafts had input features comprised of  $y_s$ ,  $D$ ,  $A_f$ ,  $\varnothing_{sb}$ ,  $\varnothing_m$ ,  $p$ ,  $q$  and  $H_s$ . As specified in AS 2870, depending on the site classification and the form of construction, the deemed-to-comply design of waffle rafts only requires the specification of the  $\varnothing_{sb}$  since the number of steel reinforcements is stipulated as one reinforcing bar for the internal beams and three reinforcing bars for the external beams. The mesh reinforcement diameter can be either a 7 or 8 mm bar on a grid of 200 mm spacing, known as SL72 or SL82. The design slab length,  $L$ , was limited to 20 m.

The DL algorithm for stiffened rafts had input features comprised of  $y_s$ ,  $D$ ,  $A_f$ ,  $n_{sb}$ ,  $\varnothing_{sb}$ ,  $n_{st}$ ,  $\varnothing_{st}$ ,  $p$ ,  $q$  and  $H_s$ . The number of reinforcements  $n_{sb}$  and  $n_{st}$  are necessary to specify the deemed-to-comply designs depending on the site classification and the form of construction. The value of  $\varnothing_m$  is a constant 7 mm bar (SL72) for  $L$  less than 18 m, which is the case in the considered lengths in this study.

The five hidden layers in Fig. 2 were observed to achieve acceptable computational efficiency and accurate results. The DL training and validation process had four stages, pre-processing, random initialisation, forward propagation, and backward propagation. The

**Table 4**  
Input features of the multi-output DL algorithm for waffle and stiffened rafts.

Input feature	Waffle raft Multi-output DL algorithm		Stiffened raft Multi-output DL algorithm	
	Minimum value	Maximum value	Minimum value	Maximum value
$y_s$	20 mm	75 mm	20 mm	75 mm
$D$	0.26 m	0.61 m	0.3 m	1.1 m
$A_f$	50 m <sup>2</sup>	300 m <sup>2</sup>	50 m <sup>2</sup>	300 m <sup>2</sup>
$n_{sb}$	–	–	2 pcs	3 pcs
$\varnothing_{sb}$	12 mm	16 mm	12 mm	16 mm
$n_{st}$	–	–	0	3 pcs
$\varnothing_{st}$	–	–	0	16 mm
$\varnothing_m$	7 mm	8 mm	–	–
$p$	2500 N/m <sup>2</sup>	7500 N/m <sup>2</sup>	2500 N/m <sup>2</sup>	7500 N/m <sup>2</sup>
$q$	6600 N/m	19500 N/m	6600 N/m	19500 N/m
$H_s$	2 m	4 m	2 m	4 m

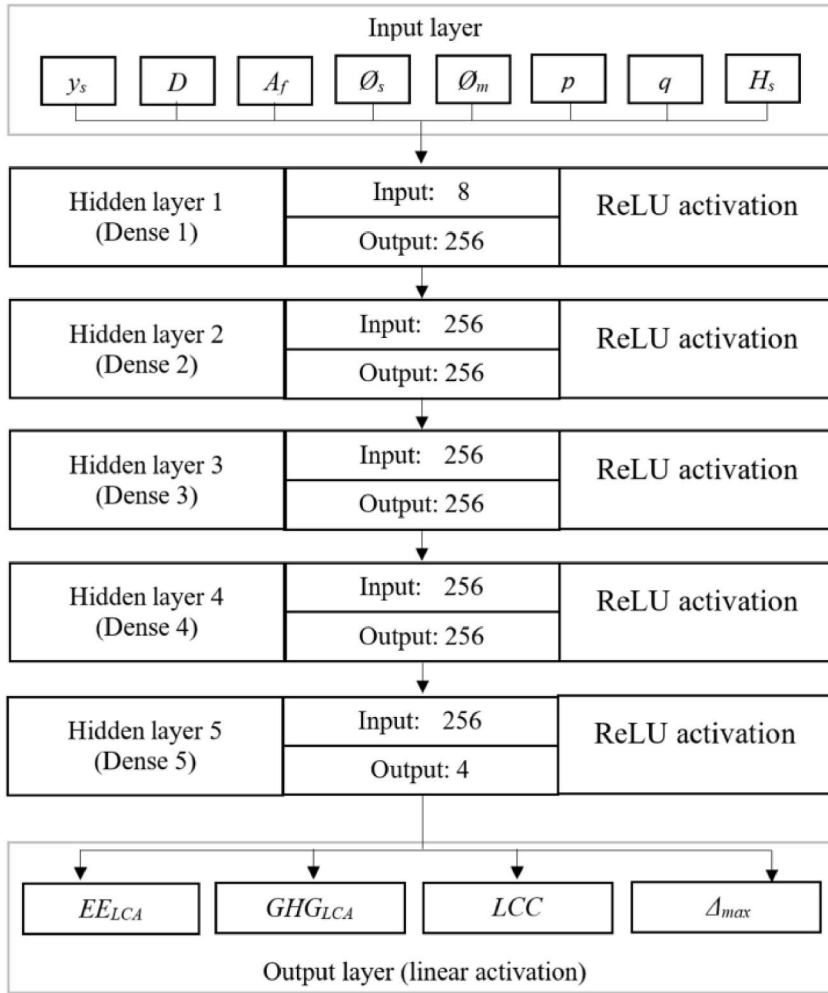


Fig. 2. Multi-output deep learning architecture.

Min-max scaling was applied to the training and validation data, equal to 2496 and 5616 data entries for the waffle raft and stiffened raft DL model. Min-max scaling is described as

$$\text{Min-max scaling} = \frac{x - x_{min}}{x_{max} - x_{min}}, \tag{7}$$

where  $x$  is the feature index,  $x_{min}$  is the minimum feature value in the dataset, and  $x_{max}$  is the maximum feature value in the dataset.

The weights of the network were randomly initialised with values close to zero. This disturbs the symmetry of the weights to enable the neurons to prevent processing error and calculate different values that will lead to acceptable results. The random initialisation by He et al. [43] was used to specify initial weights by multiplying the factor

$$\sqrt{\frac{2}{size^{DLL-1}}}, \tag{8}$$

where  $size^{DLL-1}$  is the DL layer prior to the current being analysed.

The mean squared error (MSE) was used as the loss function,  $L(y, \hat{y})$ , that is commonly used in regression models. The calculation of  $L(y, \hat{y})$  involves the squaring of the mean differences between a true value ( $y$ ) and a predicted value ( $\hat{y}$ ) by the multi-output DL model. L2 regularisation is used to prevent overfitting described by a penalty function in the second term of Equation (6),

$$L(y, \hat{y}) = \frac{1}{N} \sum_{i=0}^N (y_i - \hat{y}_i)^2 + \lambda \sum_{i=0}^N w_i^2, \tag{9}$$

where  $\lambda$  is the hyperparameter for regularisation, and  $w_i$  is a feature weight.  $\lambda$  commonly has a value greater than zero, with caution on the usage of large values of  $\lambda$  that may lead to large weights and underfitting. The value of  $N$  denotes the total number of data entries.

The Rectified Linear Units (ReLU) proposed by Nair and Hinton [44] was used in the forward propagation as an activation function described as

$$f(x) = \max(0, x_i) = \begin{cases} x_i, & \text{if } x_i \geq 0 \\ 0, & \text{if } x_i < 0 \end{cases} \quad (10)$$

where  $x_i$  is the input value.

The adaptive moment estimation or ‘‘Adam’’ optimisation by Kingma and Ba [45] was performed for the backward propagation. The Adam stochastic optimisation is widely implemented due to its efficiency. Adam optimisation method combines the momentum gradient descent and the Root Mean Square Propagation (RMSprop). The Adam optimisation algorithm is described as,

$$Vdw = \beta_1 Vdw + (1 - \beta_1)dw, \quad (11)$$

$$Vdb = \beta_1 Vdb + (1 - \beta_1)db, \quad (12)$$

$$Sdw = \beta_2 Sdw + (1 - \beta_2)dw^2, \text{ and} \quad (13)$$

$$Sdb = \beta_2 Sdb + (1 - \beta_2)db^2, \quad (14)$$

where  $Vdw$ ,  $Vdb$ ,  $Sdw$ , and  $Sdb$  are the weights and biases that are calculated in iteration or epoch,  $t$ . The initial values of  $Vdw_i$ ,  $Vdb_i$ ,  $Sdw_i$ , and  $Sdb_i$  are assigned to zero and then will be backpropagated for each weight. The calculated values of  $Vdw$ ,  $Vdb$ ,  $Sdw$ , and  $Sdb$  are then corrected and updated using the power of the current epoch,  $t$ , described below

$$w = w - \alpha \frac{V_{dw}^{corrected}}{\sqrt{S_{dw}^{corrected} + \epsilon}} = w - \alpha \frac{\frac{V_{dw}}{1 - \beta_1^t}}{\sqrt{\frac{S_{dw}}{1 - \beta_2^t} + \epsilon}}, \text{ and} \quad (15)$$

$$b = b - \alpha \frac{V_{db}^{corrected}}{\sqrt{S_{db}^{corrected} + \epsilon}} = b - \alpha \frac{\frac{V_{db}}{1 - \beta_1^t}}{\sqrt{\frac{S_{db}}{1 - \beta_2^t} + \epsilon}}. \quad (16)$$

The values of the hyperparameters were specified as  $5.0 \times 10^{-5}$  for the learning rate, 0.9, 0.999,  $5.0 \times 10^{-6}$  for the decay rates  $\beta_1$  and  $\beta_2$ , and  $\epsilon$ , and unity for the value of  $\lambda$  for all DL networks through fine-tuning.

The forward and backward propagation were implemented in a loop until the user-specified epoch was achieved. The iteration of the optimisation loop comprised of forward propagation using ReLU,  $L(y, \hat{y})$  calculation, backward propagation using Adam, and weights updating. The epoch of the final DL run was specified to be 1000. This resulted in an optimum and stable  $L(y, \hat{y})$  curve with learning periods of 404 s for waffle rafts and 990 s for stiffened rafts.

### 3. Results

The results of the calculated  $EE_{LCl}$ ,  $GHG_{LCl}$ ,  $LCC$  and  $\Delta_{max}$  using the developed multi-output DL model are discussed in this section. The validation of MOUNDS is first presented, followed by the comparison of the deemed-to-comply designs between waffle rafts and stiffened rafts.

The calculated values of  $L(y, \hat{y})$  for the training and validation sets using Equation (9) are shown in Fig. 3. The loss values of waffle rafts (Fig. 3a) and stiffened rafts (Fig. 3b) show typical learning curves, which are indicative algorithm tools that incrementally learn from training datasets. The ideal learning curve is characterised by loss values of training and validation lines that decreased to the

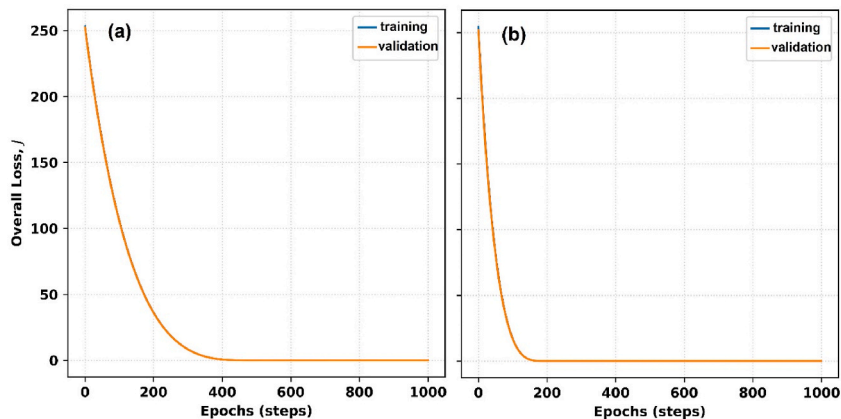


Fig. 3. Calculated loss functions,  $L(y, \hat{y})$ , of training and testing sets for (a) waffle rafts and (b) stiffened rafts.

point of stability with a minimal gap. The learning curve of the multi-output model obtained overlapping training and validation lines corresponding to an algorithm that is neither under-fitting nor overfitting, as shown in Fig. 3. The training loss for the waffle raft DL model was  $8.87 \times 10^{-04}$ , whilst the calculated validation loss was  $1.40 \times 10^{-03}$ . On the other hand, the training loss for the stiffened raft DL model was  $1.47 \times 10^{-04}$ , whilst the validation loss was  $1.31 \times 10^{-04}$ .

### 3.1. Training, validation and testing of waffle rafts

The training, validation, and testing results for the waffle raft model verify the capacity of MOUNDS to reliably predict the values of  $EE_{LCl}$ ,  $GHG_{LCl}$ ,  $LCC$  and  $\Delta_{max}$ . The  $R^2$  values for the training, validation and testing of the model ranged from 0.98 to 1.00, showing a near-perfect match between the predicted and actual values of the target outputs. Sample comparisons between the predicted and actual values of the target outputs are presented in Fig. 4.

All values of  $RMSE$  were observed to be less than one. The normalised root mean squared errors,  $RMSE_n$ , were calculated for each target output, following the equation below,

$$RMSE_n = \frac{RMSE}{x_{max} - x_{min}} = \frac{\sqrt{\frac{\sum_{i=1}^N (y_i - \hat{y}_i)^2}{N}}}{x_{max} - x_{min}}. \quad (17)$$

The values of  $RMSE_n$  were observed to be close to zero for predicting the values of  $EE_{LCl}$  and  $GHG_{LCl}$ . In predicting the values of  $LCC$ , the estimated  $RMSE_n$  were less than 1%. For the prediction of the values of  $\Delta_{max}$ , the values of  $RMSE_n$  were calculated to be less than 3%. This can be due to the non-linear relationship of the estimated value of  $\Delta_{max}$  with the input features, as opposed to that of the  $EE_{LCl}$ ,  $GHG_{LCl}$ , and  $LCC$ . The observed values of  $RMSE_n$  corroborate the reliability of the multi-output DL model for waffle rafts. The highest values of  $RMSE_n$  were calculated in the prediction of the values of  $\Delta_{max}$  (2.1–2.5%). This can be attributed to the extraction of the maximum values of  $\Delta_{max}$  in both shrinking and swelling scenarios to make the model simpler.

### 3.2. Training, validation and testing of stiffened rafts

The capability of the stiffened raft model of MOUNDS to predict the values of  $EE_{LCl}$ ,  $GHG_{LCl}$ ,  $LCC$  and  $\Delta_{max}$  was verified by comparing the actual and predicted values of the training, validation, and testing sets. Comparable to the waffle raft multi-output DL model, The  $R^2$  values for the training, validation, and testing were 1.00, showing a close to perfect match between the predicted and actual values of the target outputs. Sample comparisons between the predicted and actual values of the target outputs are presented in

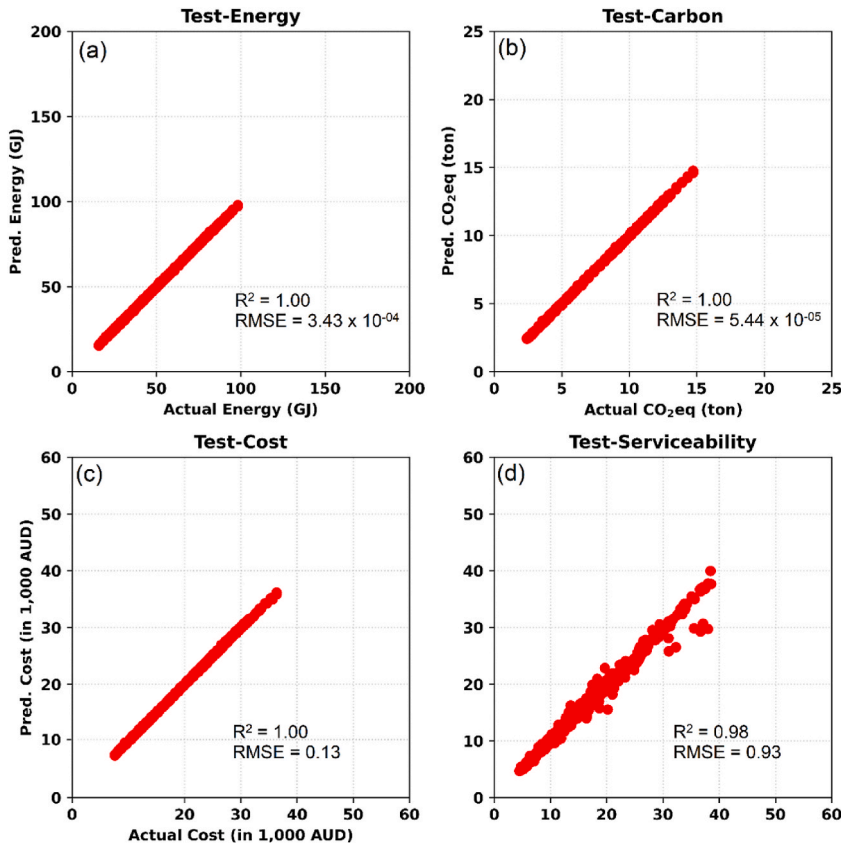


Fig. 4. Predicted and actual values of (a)  $EE_{LCl}$ , (b)  $GHG_{LCl}$ , (c)  $LCC$  and (d)  $\Delta_{max}$  for the testing of the waffle raft multi-output DL model.

Fig. 5. The values of  $RMSE$  for the stiffened raft DL model were observed to be less than one. The values of  $RMSE_n$  were observed to be close to zero for predicting the values of  $EE_{LCI}$  and  $GHG_{LCI}$ . In predicting the values of  $LCC$ , the estimated  $RMSE_n$  was approximately 0.5%. For the prediction of the values of  $\Delta_{max}$ , the values of  $RMSE_n$  were calculated to be less than 2%. These values are comparably lower than the waffle raft DL model. This may be due to the difference in the total number of data entries used, 3120 for waffle rafts and 7020 for stiffened rafts. It is a general rule in machine learning that the greater the size of the data set, the higher the accuracy of predictions. The observed values of  $RMSE_n$  further validate the reliability of the multi-output DL model for stiffened rafts.

### 3.3. Deep learning multi-output results using deemed-to-comply designs

The developed multi-output DL model for waffle rafts and stiffened rafts were used to compare the deemed-to-comply design specifications in AS 2870. The considerations involved the comparison of designs based on two forms of construction, the articulated masonry veneer (Table 5) and the articulated full masonry (Table 6) for each site class. Tables 5 and 6 present a colour heat map for each target output,  $EE_{LCI}$ ,  $GHG_{LCI}$ ,  $LCC$  and  $\Delta_{max}$ .

The comparison of  $EE_{LCI}$ ,  $GHG_{LCI}$ ,  $LCC$  between waffle rafts and stiffened rafts with an articulated masonry veneer construction shows that a stiffened raft on an H2-D site has the highest values. Contrarily, the lowest values of these target outputs were for a waffle raft on a class S site. The values of  $\Delta_{max}$  was mainly dependent on the site classification. From Tables 5 and it is evident that sites with  $H_s$  greater than or equal to 3 m (denoted by a suffix “D”) tend to have higher deformation than the sites of classifications with  $H_s$  less than 3 m.

The comparison of the target outputs between waffle rafts and stiffened rafts with an articulated full masonry had similarly revealed that a stiffened raft on H2-D site had the highest values of  $EE_{LCI}$ ,  $GHG_{LCI}$ ,  $LCC$  and  $\Delta_{max}$ . The lowest values of these target outputs were for a waffle raft on a class S site. However, deemed-to-comply designs for waffle rafts are limited and cannot accommodate H1-D, H2 and H2-D sites for construction with articulated full masonry.

## 4. Discussion

The calculated values of  $EE_{LCI}$ ,  $GHG_{LCI}$ ,  $LCC$  and  $\Delta_{max}$  based on the deemed-to-comply designs for an articulated masonry veneer had found that waffle rafts performed better than stiffened rafts in all aspects considered in this study, particularly in S, M and M-D sites. When the site becomes more reactive, the difference between the performance of waffle rafts and stiffened rafts becomes less significant.

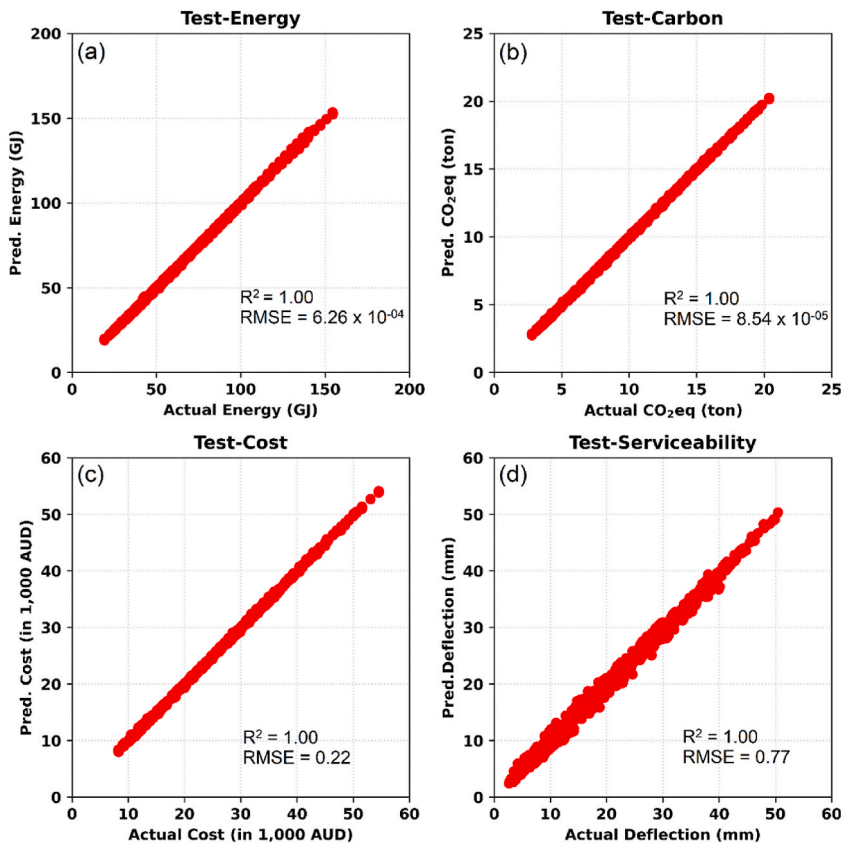


Fig. 5. Predicted and actual values of (a)  $EE_{LCI}$ , (b)  $GHG_{LCI}$ , (c)  $LCC$  and (d)  $\Delta_{max}$  for the testing of the stiffened raft multi-output DL model.

**Table 5**

Predicted values based on the deemed-to-comply designs specified in AS 2870 for waffle rafts and stiffened rafts with articulated masonry veneer construction ( $A_f = 300 \text{ m}^2$  with  $L = W = 17.3 \text{ m}$ ).

Site Class	$EE_{LCI}$ (GJ)		$GHG_{LCI}$ (ton $\text{CO}_2\text{-eq}$ )		LCC (x 1000 AUD)		$\Delta_{max}$ (mm)	
	waffle	stiffened	waffle	stiffened	waffle	stiffened	waffle	stiffened
S	59.85	66.35	9.74	11.02	23.18	23.68	4.87	19.51
M	59.7	73.77	9.78	11.75	23.21	26.02	8.87	22.76
M-D	59.57	79.03	9.8	11.72	23.28	27.35	24.84	31.41
H1	70.14	80.61	10.3	11.83	24.97	27.2	15.06	27.57
H1-D	70.35	87.32	10.34	12.65	25.28	30.12	33.87	34.68
H2	75.52	82.61	10.44	13.01	26	29.45	21.16	28.85
H2-D	76.98	111.87	11.02	14.12	27.45	36.45	34.69	36.27

**Table 6**

Predicted values based on the deemed-to-comply designs specified in AS 2870 for waffle rafts and stiffened rafts with articulated full masonry ( $A_f = 300 \text{ m}^2$  with  $L = W = 17.3 \text{ m}$ ).

Site Class	$EE_{LCI}$ (GJ)		$GHG_{LCI}$ (ton $\text{CO}_2\text{-eq}$ )		LCC (x 1000 AUD)		$\Delta_{max}$ (mm)	
	waffle	stiffened	waffle	stiffened	waffle	stiffened	waffle	stiffened
S	65.88	87.07	10.43	12.37	25.27	29.72	6.09	18.66
M	68.92	88.32	11.95	13.3	28.88	31.56	9.45	21.5
M-D	69.39	103.81	12.07	13.23	29.25	33.67	18.06	32.65
H1	78.8	114.28	11.93	14.26	29.6	37.33	15.11	25.28
H1-D	-	114.79	-	14.54	-	37.96	-	33.51
H2	-	117.45	-	15.94	-	41.33	-	28.32
H2-D	-	117.09	-	15.86	-	41.03	-	30.91

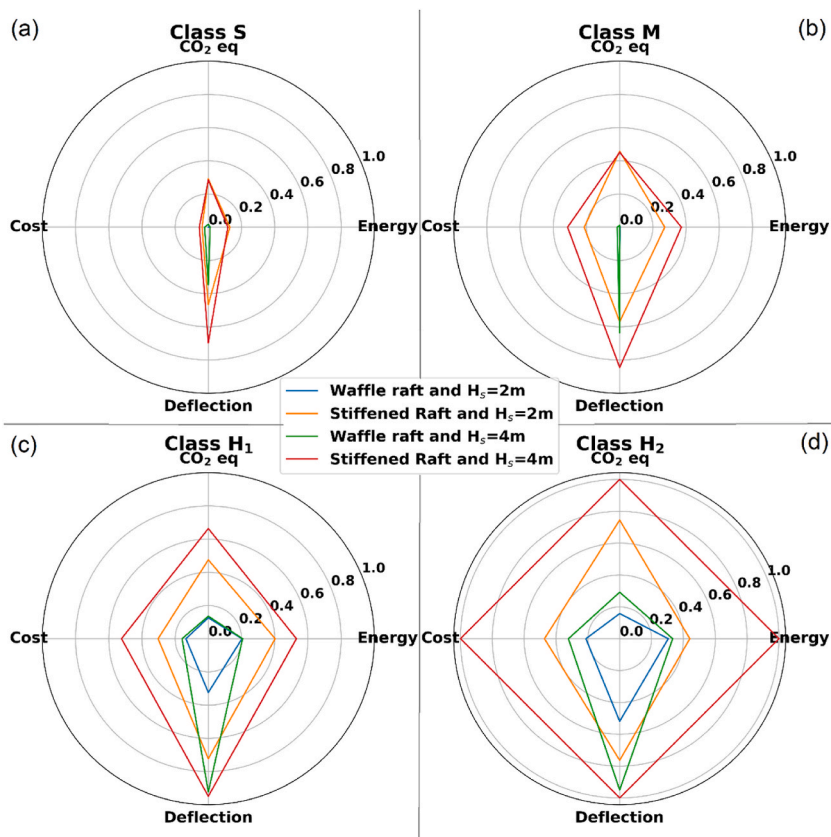


**Fig. 6.** Normalised calculated values of (a)  $EE_{LCI}$  (Energy), (b)  $GHG_{LCI}$  ( $\text{CO}_2 \text{ eq}$ ), (c) LCC (Cost) and (d)  $\Delta_{max}$  (Deflection) for waffle rafts and stiffened rafts with articulated masonry veneer based on Table 5.

A few calculated values of  $\Delta_{max}$  had exceeded the limit stipulated in AS 2870 (also shown in Table 2), which are between  $L/400$  (17,300 mm/400 = 43 mm) and 30 mm for an articulated masonry veneer construction. The waffle rafts and stiffened rafts constructed on H1-D and H2-D sites have exceeded the deflection limit (i.e., 30 mm) as expected.

The values presented in Table 5 were normalised and are presented using radar charts in Fig. 6 for a better and more insightful comparison. The relative advantages and disadvantages of waffle rafts and stiffened rafts with respect to site classifications is demonstrated in Fig. 6.

The comparison between waffle rafts and stiffened rafts with articulated masonry veneer construction shows that the relative values of  $EE_{LCI}$ ,  $GHG_{LCI}$ ,  $LCC$  and  $\Delta_{max}$  increase as the site classification becomes more reactive. The effect of deeper  $H_s$  ( $\geq 3$  m) also had a significant contribution to the increase in  $\Delta_{max}$ . Based on the stipulated designs in AS 2870, waffle rafts are a more sustainable, economical and safer option for single-detached dwellings with the lowest values of  $EE_{LCI}$ ,  $GHG_{LCI}$ ,  $LCC$  and  $\Delta_{max}$  for all site classifications.

The calculated values of  $EE_{LCI}$ ,  $GHG_{LCI}$ ,  $LCC$  and  $\Delta_{max}$  based on the deemed-to-comply designs for an articulated full masonry show similar behaviours as for the articulated masonry veneer. It is important to note that stiffened rafts can accommodate highly reactive soils with deep-seated  $H_s$  layers, unlike waffle rafts. This is due to the limited deemed-to-comply designs for waffle rafts for H1-D, H2 and H2-D sites for construction with articulated full masonry.

Most calculated values of  $\Delta_{max}$  have exceeded the limit stipulated in AS 2870-2011 (also shown in Table 2), which are the lower values between  $L/800$  (17,300 mm/800 = 22 mm) and 15 mm for an articulated masonry veneer construction. Only waffle rafts constructed on S and M sites have values below the deflection limit, which is 15 mm.

The values presented in Table 6 were also normalised and presented using radar charts in Fig. 7. It can be observed that the relative values of  $EE_{LCI}$ ,  $GHG_{LCI}$ ,  $LCC$  and  $\Delta_{max}$  increase as the site classification become more reactive. The findings also reflect that waffle rafts are a more sustainable, economical and safer option for single-detached dwellings with the lower values of  $EE_{LCI}$ ,  $GHG_{LCI}$ ,  $LCC$  and  $\Delta_{max}$  than stiffened rafts for all site classifications. However, the deemed-to-comply designs for waffle rafts in AS 2870 for full masonry constructions are limited to S, M, M-D and H1 sites [6].

## 5. Conclusions

Waffle rafts and stiffened rafts are the most common types of residential slabs in Australia, accounting for approximately 65% of the new and existing single-detached dwellings based on the Australian Housing Data by CSIRO. Due to the suitability of these residential slabs for residential structures on reactive soils, AS 2870-2011 had stipulated standard deemed-to-comply designs for both waffle rafts and stiffened rafts dependent on the site classification and form of construction. However, even though safe designs for residential slabs are important, a multi-faceted approach for a smarter and more sustainable design is imperative to alleviate the effect of changing climate. This study developed MOUNDS to predict the embodied energy, greenhouse gas emission, life cycle cost and deflection of waffle rafts and stiffened rafts. MOUNDS was also used to compare the provided deemed-to-comply designs in AS 2870 for waffle rafts and stiffened rafts to determine the optimum option.

MOUNDS was observed to accurately predict results in the training, validation and testing stages; the values of  $R^2$  for all scenarios were approximately equal to one, and the values of  $RMSE$  were below one. Furthermore, the values of  $RMSE_n$  were less than 3%. The comparison of the standard deemed-to-comply designs between waffle rafts and stiffened rafts observed that embodied energy, carbon emission, life cycle cost and deflection of residential slabs increased when the site classification was more reactive. The effect of deeper reactive soil layers also had a significant contribution to the increase in footing deflection. Based on the stipulated designs in AS 2870-2011, waffle rafts were a more sustainable, economical and safer option for single-detached dwellings with the lowest values of embodied energy, greenhouse emission, life cycle cost and deflection. However, standard deemed-to-comply designs for waffle rafts with a full masonry construction are limited to slightly and moderate reactive sites.

Most calculated values of  $\Delta_{max}$  have exceeded the limit stipulated in AS 2870-2011 (also shown in Table 2), which are the lower values between  $L/800$  (17,300 mm/800 = 22 mm) and 15 mm for an articulated masonry veneer construction. Only waffle rafts constructed on S and M sites have values below the deflection limit, which is 15 mm.

Based on the findings of this study, there is a need for design improvement of the deemed-to-comply specifications to obtain deflections within serviceability limits. This study successfully linked and predicted the complex relationship between the environmental, economic and structural design aspects of residential slabs through deep learning that is valuable in decision-making throughout the design phase. Future work related to this study includes consideration of the phases and circularity of residential slabs in their life cycle.

## Declaration of competing interest

The authors declare that they have no known competing financial interests or personal relationships that could have appeared to influence the work reported in this paper.

## Data availability

Data will be made available on request.

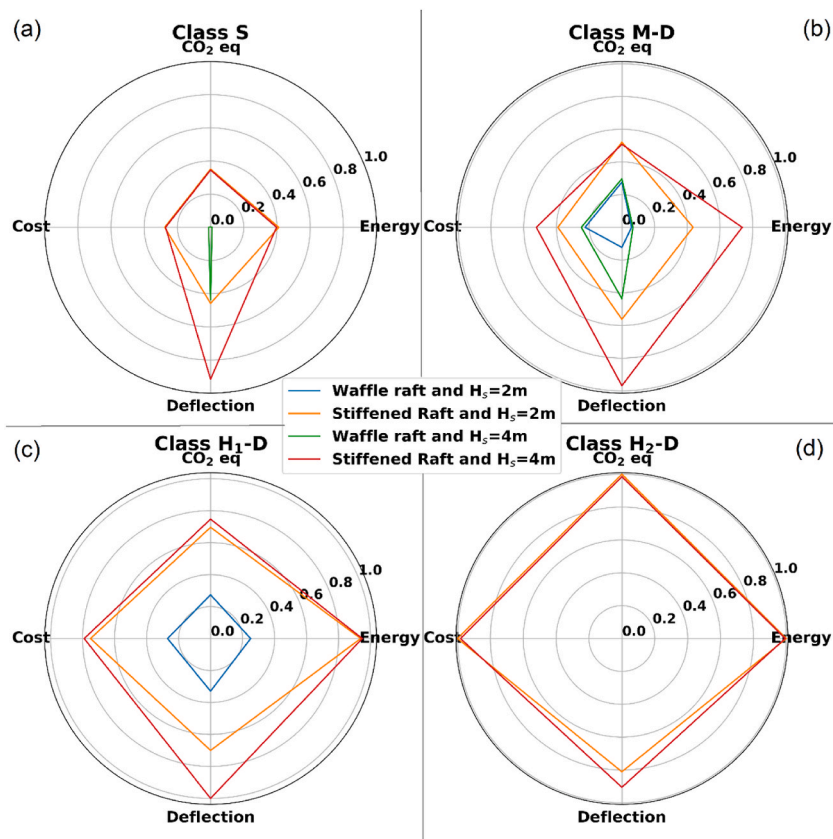


Fig. 7. Normalised calculated values of (a)  $EE_{LCI}$  (Energy), (b)  $GHG_{LCI}$  ( $CO_2$  eq), (c) LCC (Cost) and (d)  $\Delta_{max}$  (Deflection) for waffle rafts and stiffened rafts with articulated full masonry based on Table 6.

**Acknowledgements**

This work was funded in partnership with the Victorian State Government that the authors would like to acknowledge and thank.

**Appendix**

**Table A1**

Sample LCI for a waffle raft constructed on an H2 site with articulated masonry veneer ( $A_f = 300 \text{ m}^2$ ).

Item	Description	Unit	Qty	Embodied Energy, $EE_{LCI}$		Greenhouse Gas, $GHG_{LCI}$	
				Rate (GJ)	Amount (GJ)	Rate (tonCO <sub>2</sub> )	Amount (tonCO <sub>2</sub> )
<b>A</b>	<b>Materials</b>						
A1	20 MPa concrete	m3	36.37	0.1760	6.4014	0.3390	12.3299
A2	Steel reinforcement	t	1.35	48.7000	65.6415	0.0029	0.0039
A3	Waffle pod EPS	kg	35.61	0.0830	2.9554	0.0006	0.0217
A4	Sand subgrade	m3	30.00	0.2600	7.8000		
<b>B</b>	<b>Transportation</b>						
B1	Concrete	m3	36.37	0.1980	7.2016	0.0058	0.2096
B2	Steel	kg	1.35	0.0010	0.0013	0.0000	0.0000
B3	Excavator in/out	km	100.00	0.0180	1.8000	0.0013	0.1271
B4	Waffle pod (EPS) delivery	kg	35.61	0.0010	0.0356	0.0000	0.0010
<b>C</b>	<b>On-site construction</b>						
C1	Excavator (0.2 m <sup>3</sup> bucket)	h	8.82	0.1080	0.9529	0.0131	0.1158
C2	Concrete pump	h	0.79	0.5400	0.4270	0.0461	0.0365
<b>D</b>	<b>End-of-life</b>						
D1	Demolition	t	77.49	0.0070	0.5424	0.0005	0.0418
<b>Total</b>					<b>93.76</b>		<b>12.89</b>

**Table A2**Sample LCI for a stiffened raft constructed on an H2 site with articulated masonry veneer ( $A_f = 300 \text{ m}^2$ ).

Item	Description	Unit	Qty	Embodied Energy, $EE_{LCI}$		Greenhouse Gas, $GHG_{LCI}$	
				Rate (GJ)	Amount (GJ)	Rate (tonCO <sub>2</sub> )	Amount (tonCO <sub>2</sub> )
<b>A</b>	<b>Materials</b>						
A1	20 Mpa concrete	m <sup>3</sup>	46.24	0.1760	8.1390	0.3390	15.6768
A2	Steel reinforcement	t	1.60	48.7000	78.1195	0.0029	0.0047
A4	Sand subgrade	m <sup>3</sup>	30.00	0.2600	7.8000		
<b>B</b>	<b>Transportation</b>						
B1	Concrete	m <sup>3</sup>	46.24	0.1980	9.1563	0.0058	0.2665
B2	Steel	kg	1.60	0.0010	0.0016	0.0000	0.0001
B3	Excavator in/out	km	100.00	0.0180	1.8000	0.0013	0.1271
<b>C</b>	<b>On-site construction</b>						
C1	Excavator (0.2 m <sup>3</sup> bucket)	h	8.82	0.1080	0.9529	0.0131	0.1158
C2	Concrete pump	h	1.01	0.5400	0.5429	0.0461	0.0464
<b>D</b>	<b>End-of-life</b>						
D1	Demolition	t	98.52	0.0070	0.6896	0.0005	0.0532
<b>Total</b>					<b>107.20</b>		<b>16.29</b>

**Table A3**Sample LCC for a waffle raft constructed on an H2 site with articulated masonry veneer ( $A_f = 300 \text{ m}^2$ ).

Description	Qty	Unit	Rate (AUD)	Amount (AUD)
<b>Site preparation and surface treatments</b>				
Slab set-out	1	item	600.00	600.00
Mobilisation & float costs	1	item	900.00	900.00
Site levelling/vegetation removal	300	m <sup>2</sup>	2.14	642.00
Site compaction	300	m <sup>2</sup>	1.85	555.00
Installation (and removal) of fencing	69.3	linear m	42.00	2910.00
<b>Formwork and reinforcement</b>				
Steel reinforcement bars	1.0	t	2260.00	2321.00
Steel reinforcement mesh	1.1	t	2260.00	2448.00
Formwork	69.3	linear m	30.00	2078.00
Waffle pods (EPS)	219	No.	10.00	2190.00
Tradesman (placing/tie of reinforcement)	23.0	hours	63.00	1449.00
Tradesman (assembling formwork)	20.1	hours	63.00	1265.78
Labourer (assembling formwork)	7	hours	60.50	404.49
<b>Concrete pour</b>				
Concrete truck to the site	51.3	m <sup>3</sup>	200.00	10,265.80
Concrete pumping	51.3	m <sup>3</sup>	8.00	410.63
Labourer (pour, vibration, finish)	56	hours	60.50	3375.44
<b>Total</b>				<b>31,816.48</b>

**Table A4**Sample LCC for a stiffened raft constructed on an H2 site with articulated masonry veneer ( $A_f = 300 \text{ m}^2$ ).

Description	Qty	Unit	Rate (AUD)	Amount (AUD)
<b>Site preparation and surface treatments</b>				
Slab set-out	1	item	600.00	600.00
Mobilisation & float costs	1	item	900.00	900.00
Site levelling/vegetation removal	300	m <sup>2</sup>	2.14	642.00
Site compaction	300	m <sup>2</sup>	1.85	555.00
Installation (and removal) of fencing	69.3	linear m	42.00	2910.00
<b>Formwork and reinforcement</b>				
Steel reinforcement bars	2.2	t	2260.00	4922.00
Steel reinforcement mesh	0.8	t	2260.00	1883.00
Formwork	69.3	linear m	30.00	2078.00
Tradesman (placing/tie of reinforcement)	240	hours	2.14	514.00
Tradesman (assembling formwork)	32.3	hours	63.00	2068.00
<b>Concrete pour</b>				
Concrete truck to the site	71.2	m <sup>3</sup>	200.00	14,234.66
Concrete pumping	71.2	m <sup>3</sup>	8.00	569.39
Labourer (pour, vibration, finish)	77	hours	60.50	4680.42
<b>Total</b>				<b>39,088.13</b>

## References

- [1] United Nations Environment Program, Buildings and Climate Change: Summary for Decision-Makers, 2009.
- [2] B. Teodosio, Design Enhancement and Prefabrication of Raft Footings on Clayey Ground Susceptible to Reactive Soil Damage (PhD Thesis), 2020.

- [3] B. Teodosio, F. Bonacci, S. Seo, K.S.K. Baduge, P. Mendis, Multi-criteria analysis of a developed prefabricated footing system on reactive soil foundation, *Energies* 14 (2021) 7515, <https://doi.org/10.3390/en14227515>.
- [4] United Nations Environment Programme, Common carbon metric for measuring energy use & reporting greenhouse gas emissions from building operations. United Nations Environment Programme, Sustainable Buildings and Climate Initiative, Paris, Available at: <https://wedocs.unep.org/handle/20.500.11822/7922;jsessionid=105312EB13CEA1322AEAAF39F7B65B51>, 2009.
- [5] E. Pujadas-Gispert, D. Sanjuan-Delmás, A. Josa, Environmental analysis of building shallow foundations: the influence of prefabrication, typology, and structural design codes, *J. Clean. Prod.* 186 (2018) 407–417, <https://doi.org/10.1016/j.jclepro.2018.03.105>.
- [6] Standards Australia, Residential Slabs and Footings, Standard, Sydney NSW, 2011, p. 886.
- [7] B. Teodosio, K.S. Kristombu Baduge, P. Mendis, D.J. Heath, Prefabrication of substructures for single-detached dwellings on reactive soils: a review of existing systems and design challenges, *Aust. J. Civ. Eng.* 17 (2019) 120–133.
- [8] H. Yu, M. Al-Hussein, R. Nasser, R.J. Cheng, Sustainable precast concrete foundation system for residential construction, *Can. J. Civ. Eng.* 35 (2008) 190–199.
- [9] D.C. Payne, D.A. Cameron, The Walsh method of beam-on-mound design from inception to current practice, *Aust. J. Struct. Eng.* 15 (2014) 177–188.
- [10] H.G. Poulos, Piled raft foundations: design and applications, *Geotechnique* 19 (2001).
- [11] H.G. Poulos, J.P. Carter, J.C. Small, Foundations and Retaining Structures - Research and Practice 81, 2001.
- [12] A. Behnood, Soil and clay stabilization with calcium- and non-calcium-based additives: a state-of-the-art review of challenges, approaches and techniques, *Transport. Geotechnics* 17 (2018) 14–32, <https://doi.org/10.1016/j.trgeo.2018.08.002>.
- [13] H.-D. Li, C.-S. Tang, Q. Cheng, S.-J. Li, X.-P. Gong, B. Shi, Tensile strength of clayey soil and the strain analysis based on image processing techniques, *Eng. Geol.* 253 (2019) 137–148, <https://doi.org/10.1016/j.enggeo.2019.03.017>.
- [14] Y. Tao, B.P. Gautam, P.M. Pradhan, C. Hu, Characterization and reactivity of Nepali clays as supplementary cementitious material, *Case Stud. Constr. Mater.* 16 (2022), e00947, <https://doi.org/10.1016/j.cscm.2022.e00947>.
- [15] B. Teodosio, K.S.K. Baduge, P. Mendis, Relationship between reactive soil movement and footing deflection: a coupled hydro-mechanical finite element modelling perspective, *Comput. Geotech.* 126 (2020), 103720.
- [16] S.D.D.A. Gedara, P.L.P. Wasantha, B. Teodosio, J. Li, An experimental study of the size effect on core shrinkage behaviour of reactive soils, *Transport. Geotechnics* 33 (2022), 100709, <https://doi.org/10.1016/j.trgeo.2021.100709>.
- [17] J. Nelson, D.J. Miller, *Expansive Soils: Problems and Practice in*, Google Scholar, 1997.
- [18] K.M. Tran, H.H. Bui, G.D. Nguyen, DEM modelling of unsaturated seepage flows through porous media, *Comp. Part. Mech* (2021), <https://doi.org/10.1007/s40571-021-00398-x>.
- [19] T.M. Petry, D.N. Little, Review of stabilization of clays and expansive soils in pavements and lightly loaded structures—history, practice, and future, *J. Mater. Civ. Eng.* 14 (2002) 447–460.
- [20] B. Teodosio, K.S.K. Baduge, P. Mendis, Simulating reactive soil and substructure interaction using a simplified hydro-mechanical finite element model dependent on soil saturation, suction and moisture-swelling relationship, *Comput. Geotech.* 119 (2020), 103359.
- [21] E. Yaghoubi, M. Yaghoubi, M. Guerrieri, N. Sudarsanan, Improving expansive clay subgrades using recycled glass: resilient modulus characteristics and pavement performance, *Construct. Build. Mater.* 302 (2021), 124384.
- [22] L.D. Jones, I. Jefferson, *Institution of Civil Engineers Manuals Series 46*, 2012.
- [23] B. Teodosio, K.S. Kristombu Baduge, P. Mendis, A review and comparison of design methods for raft substructures on expansive soils, *J. Build. Eng.* 41 (2021), 102737, <https://doi.org/10.1016/j.jobbe.2021.102737>.
- [24] Building Research Advisory Board, *Criteria for Selection and Design of Residential Slabs-On-Ground*, National Academies Press, Washington, D.C, 1968, <https://doi.org/10.17226/9804>.
- [25] R.I. Abdelmalak, *Soil Structure Interaction for Shrink-Swell Soils “A New Design Method for Foundation Slabs on Shrink-Swell Soils*, 2007.
- [26] W. Snowden, *Design of Slab-On-Ground Foundations*, 1981.
- [27] R.L. Lytton, *Design and Performance of Material Foundations on Expansive Clay*, vol. 7, 1970.
- [28] P.F. Walsh, S.F. Walsh, *Structure/reactive-clay Model for a Microcomputer*, CSIRO Division of Building Research, 1986.
- [29] P.W. Mitchell, A simple method of design of shallow footings on expansive soil, in: *Proc. 5th Int. Conf. on Expansive Soils*, 1984.
- [30] Post Tensioning Institute, DC10.1-08: Design on PT Slabs-On-Ground, 2008.
- [31] A. Zareie, Mds.R. Amin, L.E. Amador-Jiménez, Thornthwaite moisture index modeling to estimate the implication of climate change on pavement deterioration, *J. Transport. Eng.* 142 (2016), 04016007, [https://doi.org/10.1061/\(ASCE\)TE.1943-5436.0000840](https://doi.org/10.1061/(ASCE)TE.1943-5436.0000840).
- [32] CSIRO, *Floor Construction Floor Insulation and Coverings*, 2022 [WWW Document]. Australian Housing Data. URL, <https://ahd.csiro.au/dashboards/construction/floors/>, 1.27.22.
- [33] H.G. Poulos, J.P. Carter, J.C. Small, Foundations and retaining structures-research and practice, in: *Proceedings of the International Conference on Soil Mechanics and Geotechnical Engineering*, AA Balkema Publishers, 2002, pp. 2527–2606.
- [34] ISO, ISO 14040: Environmental Management—Life Cycle Assessment—Principles and Framework, 2006.
- [35] ISO, ISO 14044: Life Cycle Assessment - Requirements and Guidelines, 2019.
- [36] Comité Européen De Normalisation, EN 15978 Sustainability of Construction Works—Assessment of Environmental Performance of Buildings—Calculation Method, CEN, Brussels, Belgium, 2012.
- [37] R.H. Crawford, A. Stephan, F. Prideaux, *Environmental Performance in Construction (EPIC) Database*, 2019.
- [38] T. Grant, *AusLCl Database Manual*, 2016.
- [39] ISO, *Buildings and Constructed Assets-Service-Life Planning, Life Cycle Costing*, 2008.
- [40] Rawlinsons, *Rawlinsons Construction Cost Guide 2019*, 2019.
- [41] V. Abaqus, 6.14 Documentation, vol. 651, Dassault Systemes Simulia Corporation, 2014.
- [42] J. Lever, M. Krzywinski, N. Altman, Points of significance: model selection and overfitting, *Nat. Methods* 13 (2016) 703–705, <https://doi.org/10.1038/nmeth.3968>.
- [43] K. He, X. Zhang, S. Ren, J. Sun, Delving deep into rectifiers: surpassing human-level performance on imagenet classification, in: *Proceedings of the IEEE International Conference on Computer Vision*, 2015, pp. 1026–1034.
- [44] V. Nair, G.E. Hinton, Rectified linear units improve restricted Boltzmann machines, *Icml* (2010).
- [45] D.P. Kingma, J. Ba, Adam: A Method for Stochastic Optimization, 2017 arXiv:1412.6980 [cs].